

Experimental study of caesium $6P_J + 6P_J \rightarrow 7P_{J'} + 6S$ energy pooling collisions and modelling of the excited atom density in the presence of optical pumping and radiation trapping

F de Tomasi^{†§}, S Milošević^{†||}, P Verkerk^{†¶}, A Fioretti^{†§}, M Allegrini^{†+},
Z J Jabbour^{†*} and J Huennekens^{†‡}

[†] Istituto Nazionale per la Fisica della Materia, Dipartimento di Fisica, Università di Pisa, Piazza
Torricelli 2, 56126 Pisa, Italy

[‡] Department of Physics, Lehigh University, 16 Memorial Drive East, Bethlehem, PA 18015,
USA

Received 11 November 1996, in final form 11 July 1997

Abstract. An experimental study of caesium energy pooling collisions, $\text{Cs}(6P_J) + \text{Cs}(6P_J) \rightarrow \text{Cs}(7P_{J'}) + \text{Cs}(6S_{1/2})$, at thermal energies, has been carried out in a capillary cell using diode laser excitation. Use of the capillary cell minimizes the effects of radiation trapping, but nonetheless, such effects still play a significant role in the analysis. Consequently, a rate equation model, which treats simultaneous effects of saturation, optical pumping, and radiation trapping, has been developed and is used to determine the $\text{Cs}(6P_J)$ atom density under these experimental conditions. The excited atom densities are combined with measured fluorescence ratios to determine rate coefficients for the caesium energy pooling process. Our values for these rate coefficients are in agreement, within combined error bars, with values we have recently obtained under very different experimental conditions.

1. Introduction

Determination of rate coefficients for collisions involving two excited atoms is fraught with difficulties. In particular, quantitative evaluation of the rate coefficient requires knowledge of both the magnitude and the spatial distribution of the excited atom density. These quantities can either be measured directly in the experiment [1], adding greatly to the complexity and cost of the set-up, or they must be evaluated using a realistic (and thus rather complicated) model, appropriate to the experiment. In addition, at atomic densities which are sufficiently high that the effects of excited atom–excited atom collisions become observable, the process of radiation trapping also becomes important. The quantitative analysis of this effect depends strongly on the geometry of the specific experiment, the type

[§] Present address: Laboratoire Aimé Cotton, CNRS II, Bat. 505, Campus d'Orsay, 91405 Orsay Cedex, France.

^{||} Permanent address: Institute of Physics, PO Box 304, HR-10000 Zagreb, Croatia.

[¶] Permanent address: Laboratoire Kastler-Brossel, Ecole Normale Supérieure, Rue Lhomond, 75231 Paris Cedex 05, France.

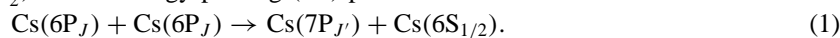
⁺ Also at: Dipartimento di Fisica della Materia e Tecnologie Fisiche Avanzate, Università di Messina, 98166 Sant'Agata-Messina, Italy.

^{*} Permanent address: Automated Production Technology Division, SOUND A147, NIST, Gaithersburg, MD 20899, USA.

of laser pumping (pulsed versus continuous wave, single mode versus broadband), the laser power (saturation effects), and the atomic-level structure (including hyperfine structure). As a result of these complications, which are not always properly taken into account, measurements of rate coefficients for excited atom–excited atom collisions typically have large error bars, and significant discrepancies exist between the results of different studies.

One purpose of this paper is to present a detailed model which can be used to determine the density of caesium atoms in the excited $6P_J$ ($J = \frac{1}{2}, \frac{3}{2}$) levels, under continuous resonant ($6S_{1/2} \rightarrow 6P_J$) excitation of caesium vapour by suitable diode lasers. The model is based on rate equations that consider the combined effects of saturation, hyperfine optical pumping, and radiation trapping. Specifically, we believe our iterative solution is the first attempt to successfully treat the interconnected effects of optical pumping and radiation trapping. Based on these results, it is apparent that measured rate coefficients will be plagued by significant errors if the excited atom density is calculated using a model which is too simple (i.e. a model which assumes that the effects of radiation trapping can be calculated without consideration of the optical pumping problem).

The results of our present model have been applied to the analysis of data from an experiment carried out at Pisa University, with the goal of determining the rate coefficients $k_{7P_{J'}} (J' = \frac{1}{2}, \frac{3}{2})$ for the energy pooling (EP) process



Preliminary values of $k_{7P_{J'}}$ for D_2 line pumping, averaged over the range of temperatures explored in this experiment, have already been reported in an earlier brief report [2]. Here, we present the complete model used in that analysis. We also give results for the rate coefficients at each temperature, as well as new data and results for D_1 pumping. In addition, we compare these results with those we obtained in a complementary, but very different, experiment carried out concurrently at Lehigh University [1]. The two experiments measure the same quantity, but with two very different approaches, each having some advantages and some drawbacks. Specifically, the present experiment is carried out using a cylindrical capillary cell similar to the cell used in [3] to reduce the problematic effects of radiation trapping. Here, the entire diameter of the capillary cell is filled with the pump laser beam. This has the advantage that the excited-atom-density spatial distribution can be considered constant with radial distance. In addition, radiation-trapping corrections are reduced since the photon escape distance is small. However, the low diode laser power, combined with the high caesium density necessary to observe the EP collisions, results in significant attenuation of the laser intensity along the cell axis, somewhat complicating the radiation-trapping geometry. Moreover, the excited-atom density is not measured, but rather is derived from the optical-pumping and radiation-trapping calculations which are described here. The strength of the Lehigh experiment [1] is that the $6P$ density and spatial distribution are directly measured. However, the cell diameter is so much larger than the laser beam diameter that the trapping calculations (which are still necessary even when the excited-atom density is known), require many higher-order escape modes (10 are used in [1]), thereby increasing the uncertainty of the results. Moreover, since the laser fills only a small fraction of the cell diameter, the hyperfine populations are assumed to be populated statistically outside the laser excitation volume. This is not completely correct because the hyperfine level populations outside the laser beam are determined by competition between diffusion of optically pumped atoms originating within the beam and the thermalizing effects of radiation trapping and wall collisions. Comparison between the two sets of experimental results shows that the measured EP rate coefficients are in agreement (within rather large statistical plus systematic uncertainties). The present results are important since they corroborate those obtained in a very different experiment, and

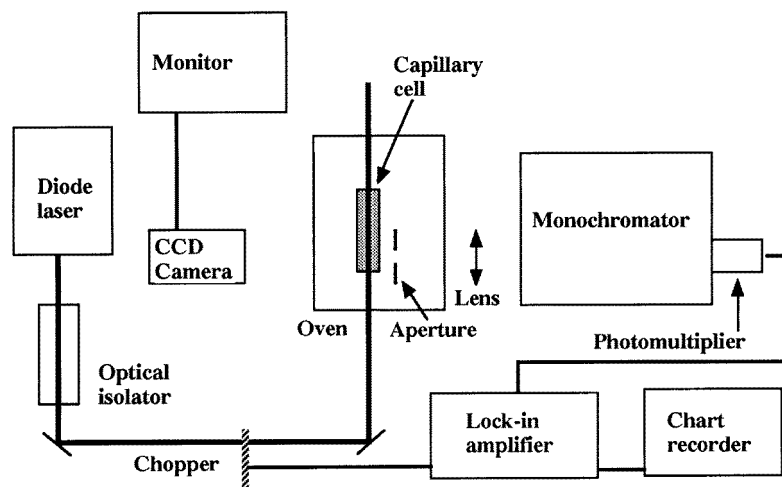


Figure 1. Schematic diagram of the experimental set-up.

thus imply that the essential physics is contained in the assumptions and approximations used in the radiation-trapping calculations of [1], and in the model results presented here. Although these results still have large uncertainties, they can provide information on atom–atom interactions at large interatomic distances, which are of particular interest in the new field of cold collisions.

One additional motivation for this work is the opportunity to study fine-structure and angular momentum effects in EP collisions. The large fine structure of the caesium $6P_J$ levels makes the study of caesium EP particularly interesting (and different from earlier studies of EP in sodium), since the combinations $6P_{3/2}+6P_{3/2}$, $6P_{1/2}+6P_{3/2}$ and $6P_{1/2}+6P_{1/2}$ are more or less resonant with various highly excited states. Specifically, our results show significant differences in the rate coefficients k_{7P_J} for the entrance channels $6P_{3/2} + 6P_{3/2}$ and $6P_{1/2} + 6P_{1/2}$.

This paper is organized as follows. Section 2 describes the set-up of the EP experiment for which the model has been developed. Section 3 recalls the rate equations for EP and presents the rate-equation model to extract the $6P_J$ atom density, for given pump conditions. Analysis and results are presented in section 4. In section 5 we present our conclusions.

2. The experiment

The set-up for the experiment is shown in figure 1. Pure caesium vapour was confined in a capillary cell, 1.8 mm inner diameter and 6 cm long. The cell was sealed after baking and evacuating with an ion pump. The cell was placed inside an oven with programmable temperature settings. The temperatures of the reservoir and capillary tube were measured with thermocouples. Caesium atomic densities were determined as a function of temperature using the formula of Nesmeyanov [4]. Caesium atoms were excited either to the $6P_{3/2}$ level using a commercial (STC) free-running single-mode laser diode, or to the $6P_{1/2}$ level using a non-commercial single-mode laser diode†, both with linewidth of roughly 20 MHz. Each laser was tuned to the transitions originating from the $F = 4$ ground-state hyperfine level and typically a laser intensity, measured at the entrance window of the cell, of 15 and

† This laser diode was kindly provided by T Yabuzaki, Kyoto University.

6 mW, respectively, was used. Because of Doppler broadening, several hyperfine levels ($F' = 5, 4, 3$) of the $6P_{3/2}$ state were excited, while the $6P_{1/2}$ state hyperfine levels were individually resolved. In this case we have selected the $F = 4 \rightarrow F' = 3$ transition. Both laser intensities were sufficient to saturate either the $6S_{1/2} \rightarrow 6P_{3/2}$ or $6S_{1/2} \rightarrow 6P_{1/2}$ transition. The laser beam propagated collinearly with the capillary tube and filled its entire diameter at the entrance window. Fine tuning of the laser frequency was achieved by variation of the diode laser current, and the resonance fluorescence signal was observed with an infrared sensitive CCD camera. This camera also helped during the alignment of the laser beam along the axis of the capillary tube, since the propagation of the laser beam through the capillary was easily observed on the monitor, even at room temperature. Scattered light could be minimized in this way. Changes in the spatial distribution of the $6P_J$ emission were monitored as well. For example, at low atom densities ($5 \times 10^{12} \text{ cm}^{-3}$) and maximum laser power, the entire volume of the capillary tube fluoresced homogeneously. However, if the laser power was decreased by means of a neutral density filter, the $6P_J$ emission decreased sharply as a function of distance along the beam path.

Fluorescence from a small volume, selected by a slit-shaped mask of $500 \mu\text{m}$ width near the entrance window of the capillary cell, was imaged onto the entrance slit of a $\frac{1}{4}$ m monochromator having typical slit widths of $450 \mu\text{m}$. This gave spectral resolution sufficient to separate the $7P_{3/2}$ and $7P_{1/2}$ fine-structure components, responsible for the 455.7 nm ($7P_{3/2} \rightarrow 6S_{1/2}$) and 459.4 nm ($7P_{1/2} \rightarrow 6S_{1/2}$) emission, respectively. At atom densities above 10^{13} cm^{-3} , blue light from that region was easily seen by the naked eye. Spatially, it appeared as a cone peaking in the propagation direction of the laser beam, since the excited-atom density dropped off with distance along the cell at these high atom densities. However, due to the slit-shaped mask described above, only the base of that cone, corresponding to the region near the cell entrance window where the blue fluorescence filled the full cell diameter, was imaged onto the monochromator entrance slit. Light was detected with a photomultiplier (Hamamatsu R955). The diode laser beam was chopped and lock-in detection was used. Signals were recorded with an X - Y recorder. Neutral density filters were used in the fluorescence path since resonance and EP fluorescence intensities differed by factors of 10^6 - 10^8 (see [2] figure 2). Therefore care was taken in the calibration of filters at different wavelengths. The spectral response of the system was measured by means of a calibrated tungsten ribbon lamp [5]. The apparatus was found to be much more sensitive in the blue part of the spectrum (450 nm) than in the near infrared (850 nm). In addition, from 852.3 nm (D_2 line) towards 894.6 nm (D_1 line) the sensitivity sharply decreased. This prevented us from observing $6D \rightarrow 6P$ fluorescence (876.4 nm), at lower atom densities where $7P \rightarrow 6S$ fluorescence could already be observed.

The procedure of the measurement was the following. First the monochromator was set to the $6P_J \rightarrow 6S$ transition and the laser was tuned to observe and record the maximum signal from the photomultiplier. This laser frequency coincides with the maximum absorption monitored by observing the attenuation over the entire length of the cell. Then the monochromator was tuned to the $7P_{J'} \rightarrow 6S$ transition and, in case of drift, the laser frequency was again tuned to the maximum of the absorption coefficient. The $7P_{J'} \rightarrow 6S$ fluorescence was then recorded. The same procedure was repeated at several temperatures (and therefore different atom densities).

3. Theory

Figure 2 shows the processes considered in this work and the hyperfine levels relevant to the $6P_J$ state excitation. The effective radiative rates are represented by downward straight

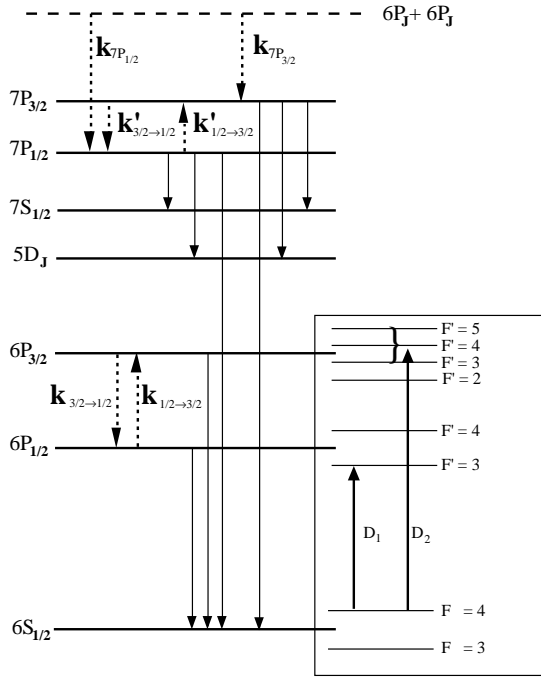


Figure 2. Schematic diagram of caesium energy levels relevant to the present experiment. Full downward arrows represent radiative transitions, broken arrows represent collisional processes.

arrows, $k_{3/2 \rightarrow 1/2}$ and $k_{1/2 \rightarrow 3/2}$ indicate 6P level fine-structure mixing, $k'_{3/2 \rightarrow 1/2}$ and $k'_{1/2 \rightarrow 3/2}$ indicate 7P level fine-structure mixing, and $k_{7P_{1/2}}$ and $k_{7P_{3/2}}$ represent EP rate coefficients.

3.1. Rate equations for EP

The complete rate equation for the population of the $7P_{J'}$ level reads:

$$\frac{dn_{7P_{J'}}}{dt} = k_{7P_{J'}}^{(3/2)} \frac{n_{6P_{3/2}}^2}{2} + k_{7P_{J'}}^{(1/2, 3/2)} n_{6P_{3/2}} n_{6P_{1/2}} + k_{7P_{J'}}^{(1/2)} \frac{n_{6P_{1/2}}^2}{2} + k'_{J'' \rightarrow J'} n_{7P_{J''}} n_{6S_{1/2}} + \sum_{n''L''} \Gamma_{n''L'' \rightarrow 7P_{J'}}^{\text{eff}} n_{n''L''} - \sum_{n''L''} \Gamma_{7P_{J'} \rightarrow n''L''}^{\text{eff}} n_{7P_{J'}} - k'_{J'' \rightarrow J'} n_{7P_{J''}} n_{6S_{1/2}}. \quad (2)$$

Here n_{nL_J} is the density in the atomic level nL_J , $k_{7P_{J'}}^{(3/2)}$, $k_{7P_{J'}}^{(1/2, 3/2)}$, and $k_{7P_{J'}}^{(1/2)}$ are EP rate coefficients connected with the different entrance channels $6P_{3/2} + 6P_{3/2}$, $6P_{1/2} + 6P_{3/2}$ and $6P_{1/2} + 6P_{1/2}$, respectively, $k'_{J'' \rightarrow J'}$ and $k'_{J' \rightarrow J''}$ are fine structure mixing rate coefficients for the 7P levels, and $\Gamma_{n''L'' \rightarrow nL}$ is the radiative rate from level $n''L''$ to level nL . Due to radiation trapping, these rates must often be expressed as effective radiative rates Γ^{eff} . The first sum over $n''L''$ represents cascade radiation contributions from higher-lying levels, while the second corresponds to radiative decay to lower levels ($5D_{3/2, 5/2}$, $7S_{1/2}$, $6S_{1/2}$) which is the dominant depletion process. In the absence of trapping, $\sum_{n''L''} \Gamma_{7P_{J'} \rightarrow n''L''}^{\text{eff}}$ is the sum of the Einstein spontaneous emission rates for transitions to all lower states.

In this experiment, the laser only excites the $6P_{1/2}$ level or the $6P_{3/2}$ level, but not both. In equation (2) we consider all three entrance channels $6P_{1/2} + 6P_{1/2}$, $6P_{1/2} + 6P_{3/2}$ and $6P_{3/2} + 6P_{3/2}$, since fine-structure changing collisions, such as

$$\text{Cs}(6P_{3/2}) + \text{Cs}(6S_{1/2}) \rightleftharpoons \text{Cs}(6P_{1/2}) + \text{Cs}(6S_{1/2}), \quad (3)$$

can result in population of both levels. However, under the present experimental conditions, fine-structure mixing is relatively weak, even at our highest densities (i.e. $(k'_{3/2 \rightarrow 1/2} = 3.86 \times 10^{-10} \text{ cm}^3 \text{ s}^{-1} [6]) \times n_{6S_{1/2}} \ll (\Gamma_{7P_{j'}} = 6.45 \times 10^6, 9.07 \times 10^6 \text{ s}^{-1} [7])$ for 7P and $(k_{3/2 \rightarrow 1/2} = 1.12 \times 10^{-10} \text{ cm}^3 \text{ s}^{-1} [8]) \times n_{6S_{1/2}} \ll \Gamma_{6P_j}^{\text{eff}}$ for 6P). Thus we can neglect the $6P_{1/2} + 6P_{1/2}$ and $6P_{1/2} + 6P_{3/2}$ entrance channels for laser pumping of the $6S_{1/2} \rightarrow 6P_{3/2}$ (D_2) transition (and similarly we can neglect the $6P_{3/2} + 6P_{3/2}$ and $6P_{1/2} + 6P_{3/2}$ channels for $6S_{1/2} \rightarrow 6P_{1/2}$ (D_1) pumping), as long as the EP rate coefficients for the three channels are not too different from each other. We can also safely neglect the terms involving $k'_{j' \rightarrow j''}$ and $k'_{j'' \rightarrow j'}$ in equation (2). Finally, we neglect the cascade terms $\Gamma_{n''L'' \rightarrow 7P_{j'}}^{\text{eff}}$ in equation (2). Later we will see that this last assumption is reasonable, except for the possible cascade contribution from 8S in the case of D_2 pumping. (We will return to the discussion of this situation in section 4.) With these approximations, we can solve equation (2) in steady state as

$$k_{7P_{j'}}^{(J)} = 2 \times \frac{\sum_{n''L''} \Gamma_{7P_{j'} \rightarrow n''L''}^{\text{eff}} n_{7P_{j'}}}{[n_{6P_j}]^2}. \quad (4)$$

Measured fluorescence intensities are given by

$$I_{7P_{j'} \rightarrow 6S_{1/2}} = h\nu_{7P_{j'} \rightarrow 6S_{1/2}} \epsilon_{7P_{j'} \rightarrow 6S_{1/2}} n_{7P_{j'}} \Gamma_{7P_{j'} \rightarrow 6S_{1/2}}^{\text{eff}} V \frac{\Omega}{4\pi} \quad (5)$$

$$I_{6P_j \rightarrow 6S_{1/2}} = h\nu_{6P_j \rightarrow 6S_{1/2}} \epsilon_{6P_j \rightarrow 6S_{1/2}} n_{6P_j} \Gamma_{6P_j \rightarrow 6S_{1/2}}^{\text{eff}} V \frac{\Omega}{4\pi} \quad (6)$$

where ϵ is the spectral response of the detection system, ν is the emission frequency, Ω is the collection solid angle, and V is the fluorescence volume. Extracting $n_{7P_{j'}}$ and n_{6P_j} from (5) and (6), and substituting into (4), we obtain for the rate coefficients

$$k_{7P_{j'}}^{(J)} = 2 \times \frac{(I_{7P_{j'} \rightarrow 6S_{1/2}} / \epsilon_{7P_{j'} \rightarrow 6S_{1/2}}) \lambda_{7P_{j'} \rightarrow 6S_{1/2}} \sum_{n''L''} \Gamma_{7P_{j'} \rightarrow n''L''}^{\text{eff}} \Gamma_{6P_j \rightarrow 6S_{1/2}}^{\text{eff}}}{(I_{6P_j \rightarrow 6S_{1/2}} / \epsilon_{6P_j \rightarrow 6S_{1/2}}) \lambda_{6P_j \rightarrow 6S_{1/2}} \Gamma_{7P_{j'} \rightarrow 6S_{1/2}}^{\text{eff}} n_{6P_j}}. \quad (7)$$

In order to determine $k_{7P_{j'}}^{(J)}$ we measure the intensity ratio of EP and resonance fluorescence versus atom density. We obtain the excited-atom density n_{6P_j} and effective radiative rates of the $6P_j \rightarrow 6S_{1/2}$ transitions by modelling the rate equations as described in the next subsection. $\Gamma_{7P_{j'} \rightarrow n''L''}^{\text{eff}}$ values are calculated using radiation trapping theory [9, 10] and natural radiative rates taken from the literature [7].

3.2. Modelling of the $6P_j$ atom density

As can be seen from either equation (4) or (7), the measurement of the rate coefficients for caesium EP collisions requires precise knowledge of the density of atoms in the $6P_j$ states. In addition, values of the effective radiative rate for the $6P_j \rightarrow 6S_{1/2}$ fluorescence must also be known. Thus relative populations in the hyperfine levels of the ground state should be measured or calculated. Because additional probe lasers at suitable wavelengths were not available, we rely on calculations of these populations taking into account all relevant physical processes. We exploit the experimental fact that the resonance fluorescence saturates as a function of laser intensity (at least near the cell entrance window where the fluorescence is observed), so that the exact value of laser intensity should not be critical for the determination of the 6P population. Our model takes into account: (i) the fact that the laser linewidth (~ 20 MHz) is much smaller than the Doppler width (~ 400 MHz), so that only a small fraction of the velocity distribution is excited; (ii) wall collisions, which depopulate excited levels and

thermalize the populations in the hyperfine levels of the ground state; (iii) hyperfine optical pumping in the ground state during the atomic transit time ($\sim 8 \mu\text{s}$) across the cell; (iv) the $6P_{3/2}$ state hyperfine structure, because optical pumping is different for excitation of each $6P_{3/2}$ state hyperfine level; (v) radiation trapping, which is not negligible for either the $6P_{1/2}$ or the $6P_{3/2}$ fluorescence (this last effect influences optical pumping, which in turn affects trapping, so that the two effects must be handled together).

To model optical pumping, we use the fact that the rate of wall collisions is much higher than the interatomic collision rate, so we can neglect the latter for the purpose of calculating the $6P_J$ density, n_{6P_J} . This assumption is justified because the average atomic transit time through the cell, in the transverse direction, is much shorter than the mean time between collisions. (For a caesium atom of mass $M = 2.21 \times 10^{-25}$ kg, with RMS velocity in the plane perpendicular to the cell axis $v_T = \sqrt{2kT/M}$, the transit time across a cylindrical cell of radius $R = 0.9$ mm is $\sim 8 \mu\text{s}$ at $T = 400$ K. The relaxation rate for wall collisions is related to this, and is given by [11])

$$\gamma_w = 1.78 \frac{v_T}{\pi R} = 0.567 \frac{v_T}{R}. \quad (8)$$

On the other hand, a typical mean time between interatomic collisions is given by $(\sigma_T n v)^{-1} \sim 40 \mu\text{s}$, where $n \sim 6.6 \times 10^{13} \text{ cm}^{-3}$ at $T = 400$ K, v is the mean collision velocity between two caesium atoms ($v = \sqrt{16kT/\pi M}$), and $\sigma_T \sim 10^{-14} \text{ cm}^2$ is a reasonable upper limit for the geometrical cross section. Thus, interatomic collisions are only a minor perturbation in determining the atomic distribution over ground and excited levels.)

The wall relaxation rate given in equation (8) must be modified when we also consider collisions with the cell entrance window. Our observation zone is a cylinder of radius $R = 0.9$ mm and length $L = 0.5$ mm. However, wall relaxation collisions only occur at the entrance window and the side walls; the ‘back’ surface of the cylinder is open to the cell interior. An extension of the model presented in [11] shows that the correct wall relaxation rate for our geometry (i.e. including the contributions from collisions with the entrance window) is given by

$$\gamma_w = \left(\frac{0.567}{R} + \frac{0.282}{L} \right) v_T. \quad (9)$$

Another important assumption of the model is that the velocity distribution in the different hyperfine levels is taken to be thermalized. This assumption is justified when radiation trapping and the long-range velocity exchanging resonant process

$$6S_{1/2}(v) + 6P_J(v') \rightleftharpoons 6S_{1/2}(v') + 6P_J(v) \quad (10)$$

cause complete thermalization, as recently studied experimentally [12]. Under these assumptions we can write the rate equations for an ensemble of thermally populated states, in a model similar to that of [13]. The main difference of the present analysis is the inclusion of the hyperfine structure of the $6P_J$ levels and of radiation trapping.

Rate equations for the densities in the excited levels $6P_J(F')$, the ground-state hyperfine level which primarily interacts with the laser ($6S_{1/2}(F = 4)$), and the other ground-state hyperfine level ($6S_{1/2}(F = 3)$), which is only weakly coupled by the laser, are given by the following:

$$\begin{aligned} \dot{n}_{6P_J(F')} = & - \sum_F B_{6P_J(F') \rightarrow 6S_{1/2}(F)} I_L \left(n_{6P_J(F')} - \frac{g_{F'}}{g_F} n_{6S_{1/2}(F)} \right) \\ & - \left(\sum_F \Gamma_{6P_J(F') \rightarrow 6S_{1/2}(F)}^{\text{eff}} + \gamma_w \right) n_{6P_J(F')} \end{aligned} \quad (11)$$

$$\begin{aligned} \dot{n}_{6S_{1/2}(F=4)} = & \sum_{F'} B_{6P_J(F') \rightarrow 6S_{1/2}(F=4)} I_L \left(n_{6P_J(F')} - \frac{g_{F'}}{g_{F=4}} n_{6S_{1/2}(F=4)} \right) \\ & + \sum_{F'} \Gamma_{6P_J(F') \rightarrow 6S_{1/2}(F=4)}^{\text{eff}} n_{6P_J(F')} + \gamma_w \left(\frac{ng_{F=4}}{g_{F=3} + g_{F=4}} - n_{6S_{1/2}(F=4)} \right) \end{aligned} \quad (12)$$

$$\begin{aligned} \dot{n}_{6S_{1/2}(F=3)} = & \sum_{F'} B_{6P_J(F') \rightarrow 6S_{1/2}(F=3)} I_L \left(n_{6P_J(F')} - \frac{g_{F'}}{g_{F=3}} n_{6S_{1/2}(F=3)} \right) \\ & + \sum_{F'} \Gamma_{6P_J(F') \rightarrow 6S_{1/2}(F=3)}^{\text{eff}} n_{6P_J(F')} + \gamma_w \left(\frac{ng_{F=3}}{g_{F=3} + g_{F=4}} - n_{6S_{1/2}(F=3)} \right). \end{aligned} \quad (13)$$

Here $\dot{n}_{nL_J(F)}$ is the time rate of change of the $nL_J(F)$ hyperfine level number density, n is the total caesium atom density, and I_L is the laser intensity. In addition, γ_w is given by equation (9) and $g_F = (2F + 1)$ is the statistical weight of level F . In order to simplify the expression for the level populations we introduce the following definitions:

$$\beta_{F'F} \equiv \frac{g_{F'}}{g_F} \frac{B_{6P_J(F') \rightarrow 6S_{1/2}(F)} I_L}{\sum_{F''} (B_{6P_J(F') \rightarrow 6S_{1/2}(F'')} I_L + \Gamma_{6P_J(F') \rightarrow 6S_{1/2}(F'')}^{\text{eff}}) + \gamma_w} \quad (14)$$

$$\begin{aligned} Q \equiv & \sum_{F'} \beta_{F'4} \left(B_{6P_J(F') \rightarrow 6S_{1/2}(F=3)} I_L + \Gamma_{6P_J(F') \rightarrow 6S_{1/2}(F=3)}^{\text{eff}} \right. \\ & \left. + \frac{\gamma_w g_{F=3}}{g_{F=3} + g_{F=4}} \right) + \frac{\gamma_w g_{F=3}}{g_{F=3} + g_{F=4}} \end{aligned} \quad (15)$$

$$\begin{aligned} R \equiv & \sum_{F'} \beta_{F'3} \left(B_{6P_J(F') \rightarrow 6S_{1/2}(F=4)} I_L + \Gamma_{6P_J(F') \rightarrow 6S_{1/2}(F=4)}^{\text{eff}} \right. \\ & \left. + \frac{\gamma_w g_{F=4}}{g_{F=3} + g_{F=4}} \right) + \frac{\gamma_w g_{F=4}}{g_{F=3} + g_{F=4}}. \end{aligned} \quad (16)$$

(The physical significance of these terms is the following: $\beta_{F'F}$ is just the ratio of population in the excited sublevel $6P_J(F')$ to that in the ground-state sublevel $6S_{1/2}(F)$ that would be obtained if we solved equation (11) in steady state using the assumption that the laser couples to only one hyperfine level (F) of the ground state. Substituting this ratio into equations (12) and (13), we see that Q and R represent effective transfer rates between the ground state sublevels, including both hyperfine optical pumping and relaxation through wall collisions.)

Taking into account the constraint that the total number of atoms is conserved, i.e. $\sum_{F'} n_{6P_J(F')} + n_{6S_{1/2}(F=4)} + n_{6S_{1/2}(F=3)} = n$, we may solve equations (11)–(13) in steady state to yield

$$n_{6S_{1/2}(F=4)} = \frac{Rn}{R(1 + \sum_{F'} \beta_{F'4}) + Q(1 + \sum_{F'} \beta_{F'3})} \quad (17)$$

$$n_{6S_{1/2}(F=3)} = \frac{Qn_{6S_{1/2}(F=4)}}{R} \quad (18)$$

$$n_{6P_J(F')} = \sum_F \beta_{F'F} n_{6S_{1/2}(F)}. \quad (19)$$

For a laser frequency ω_L , the stimulated emission rates are given by

$$\begin{aligned} B_{6P_J(F') \rightarrow 6S_{1/2}(F)}(\omega_L) = & \frac{\lambda^3}{8\pi hc} \frac{\Gamma_{6P_J(F') \rightarrow 6S_{1/2}(F)} \Gamma}{\Delta \sqrt{\pi}} \\ & \times \int_{-\infty}^{+\infty} \frac{\exp[-(\omega - \omega_{6P_J(F') \rightarrow 6S_{1/2}(F)})^2 / \Delta^2]}{(\omega_L - \omega)^2 + (\Gamma/2)^2} d\omega \end{aligned} \quad (20)$$

where λ is the transition wavelength, h and c are Planck's constant and the speed of light, respectively, $\Gamma_{6P_J(F') \rightarrow 6S_{1/2}(F)}$ is the natural radiative rate, and $\omega_{6P_J(F') \rightarrow 6S_{1/2}(F)}$ is the line centre frequency of the hyperfine transition. Here $\Delta = \frac{2\pi}{\lambda} \sqrt{\frac{2kT}{M}}$ is a measure of the Doppler width, and $\Gamma = \Gamma_{6P_J \rightarrow 6S_{1/2}} + \Gamma_L + \Gamma_{SB}$ is the Lorentzian line width (FWHM). The three contributions to the Lorentzian width represent natural broadening ($\Gamma_{6P_J \rightarrow 6S_{1/2}} = 3.26 \times 10^7 \text{ s}^{-1}$ and $2.89 \times 10^7 \text{ s}^{-1}$ for the D₂ and D₁ lines, respectively [7]), the laser linewidth ($\Gamma_L = 1.26 \times 10^8 \text{ s}^{-1}$), and self-broadening ($\Gamma_{SB} = 9.48 \times 10^{-7} n \text{ s}^{-1}$ and $4.71 \times 10^{-7} n \text{ s}^{-1}$ for D₂ [14] and D₁ [15], respectively). Hyperfine transition rates $\Gamma_{6P_J(F') \rightarrow 6S_{1/2}(F)}$ are taken from [16].

In the presence of radiation trapping, the radiative rates must be considered as dependent on the ground- and excited-state hyperfine level populations. The various spontaneous emission coefficients are multiplied by the trapping factors g_F^T lowering the transition probability:

$$\Gamma_{6P_J(F') \rightarrow 6S_{1/2}(F)}^{\text{eff}} = g_F^T \Gamma_{6P_J(F') \rightarrow 6S_{1/2}(F)}. \quad (21)$$

The g_F^T trapping factors can be calculated using the standard theory of radiation trapping as given by Holstein in the formulation developed by Molisch *et al* [9, 10]. They depend on F because the two sublevels of the ground state are sufficiently separated in frequency that photons emitted on transitions to $F = 3$ are highly unlikely to be reabsorbed by atoms in $F = 4$ and vice versa, at these temperatures.

In the above rate equations all radiative rates are effective rates. As a consequence, an analytical solution of equations (17)–(19) is impossible. However, it is possible to solve these equations using an iterative approach. In steady state, for a given distribution of atomic population in the various hyperfine levels, and considering the populations independent of the radial position in the cell, we can write the absorption coefficient for the transitions $6S_{1/2}(F) \rightarrow 6P_J$ starting from the hyperfine level F , as a superposition of unresolved Doppler lines:

$$k_F(\omega) = \hbar\omega \sum_{F'} B_{6P_J(F') \rightarrow 6S_{1/2}(F)}(\omega) \left[\frac{g_{F'}}{g_F} n_{6S_{1/2}(F)} - n_{6P_J(F')} \right]. \quad (22)$$

To calculate the trapping factor, the maximum absorption coefficient k_F^{max} is calculated as in [1]. From equations (17)–(19), we determine populations in the absence of trapping and use them to calculate approximate trapping factors. The populations are then recalculated using the new values of Γ^{eff} in equations (17)–(19); this procedure is iterated until a variation of less than 1% in the populations is obtained. When the process has converged, we calculate trapping factors for the $7P_{J'} \rightarrow 6S_{1/2}(F)$ transitions. The reductions in the $7P \rightarrow 6S$ transition probabilities are less severe than those for $6P \rightarrow 6S$, and the changes from the natural radiative rates for the $7P \rightarrow 6S$ transitions range from less than 1% at the lowest temperature to 60% at the highest temperature. Since the $6P_{3/2}$, $7P_{1/2}$ and $7P_{3/2}$ state hyperfine structures are not resolved due to Doppler broadening, we use a single trapping factor to describe emission from all hyperfine levels within each of those states to a given ground-state hyperfine level $6S_{1/2}(F)$. Thus we suppose that emitted photons see the same absorption coefficient regardless of the initial hyperfine level. For $6P_{1/2}$, the hyperfine levels are sufficiently separated that individual $F' \rightarrow F$ trapping factors must be calculated. In the following, we will always implicitly assume that D₁ line trapping factors refer to $F' = 3$.

Because the laser beam fills the entire cell diameter, we only consider the lowest mode for the trapping problem. (In [1], a 10-mode expansion was necessary because, in that case, the laser beam diameter was much smaller than the cell diameter.) Generally, trapping calculations of this type are based upon some 'ideal' geometry such as a sphere,

an infinite cylinder, or an infinite slab. Such an approximation is required in the present case since analytic formulae for the trapping factors are needed to keep the computation time manageable in our iterative solution. Here we can calculate g_F^T from the infinite cylinder approximation [9], using $k_F^{\max} R$ as the input parameter, with $R = 0.9$ mm being the cell radius. However, the infinite cylinder is not a very good match to our geometry, because we observe fluorescence from a region close to the cell entrance window where the smallest photon escape distance is about half of the cell radius. Thus the infinite cylinder approximation clearly overestimates the trapping since light can also escape from the cell entrance window. In the opposite extreme, a sphere of radius $L/2$, where $L = 0.5$ mm is the length of the observation zone, must represent a lower bound on the trapping since all photon escape distances from the centre of the observation zone are at least as great as $L/2$ [9]. Here we have chosen to model the trapping geometry as an infinite slab of thickness equal to L , with the input parameter to the trapping calculations being $k_F^{\max} L$ [10]. We believe the slab represents a good compromise for the geometry since the neglect of escape out of the side walls is partially compensated in the slab calculations by inclusion of escape out of the ‘back’ slab face into the cell interior (escape in that direction does not occur effectively since photons leaving the observation zone through that ‘surface’ are replaced by other photons entering through the same surface from further down the length of the cell). The slab calculations yield trapping factors g_F^T which are approximately a factor of 2 smaller and a factor of 2 larger than those obtained from the sphere and infinite cylinder formulae, respectively. We believe the uncertainty in the g_F^T factors is much less than a factor of two, since the sphere and cylinder are unrealistic extreme cases. However, the uncertainty in the trapping factors is certainly one of the most important sources of uncertainty in the EP rate coefficients derived from our experimental data.

We note here that the calculation of the level populations using this model of optical pumping and radiation trapping depends on the laser frequency. The latter was not measured in our experiment, but rather it was set to maximize the $6P_J \rightarrow 6S_{1/2}$ fluorescence. Experimentally this frequency also maximizes the absorption. Thus our model calculations were carried out as a function of laser frequency in order to determine the frequency that maximizes these signals. It turns out from the model that fluorescence and absorption are maximized at the same frequency (see figure 3(b)). Once this frequency was found, all further calculations were based upon the assumption that this was the laser frequency actually used in the experimental measurements of $I_{6P_J \rightarrow 6S_{1/2}}$ and $I_{7P_{J'} \rightarrow 6S_{1/2}}$. The laser frequency dependence of the level populations, trapping factors and the absorption coefficient are presented in the next section.

4. Results and discussion

For $6P_{3/2}$ excitation at different temperatures, we have calculated the various parameters entering into the determination of the EP rate coefficients, i.e.

$$n_{6P_{3/2}}, \quad \Gamma_{6P_{3/2} \rightarrow 6S_{1/2}(F)}^{\text{eff}} \quad \text{and} \quad G_{7P_{J'}} \equiv \frac{\sum_{n''L''} \Gamma_{7P_{J'} \rightarrow n''L''}^{\text{eff}}}{\Gamma_{7P_{J'} \rightarrow 6S_{1/2}}^{\text{eff}}} \bigg/ \frac{\sum_{n''L''} \Gamma_{7P_{J'} \rightarrow n''L''}}{\Gamma_{7P_{J'} \rightarrow 6S_{1/2}}}$$

as a function of laser detuning. The effective transition probability for the $6P_J$ level is calculated by averaging the effective hyperfine transition probabilities, weighted with the populations of the hyperfine sublevels:

$$\Gamma_{6P_J \rightarrow 6S_{1/2}}^{\text{eff}} = \frac{\sum_{F, F'} \Gamma_{6P_J(F') \rightarrow 6S_{1/2}(F)}^{\text{eff}} n_{6P_J(F')}}{n_{6P_J}} \quad (23)$$

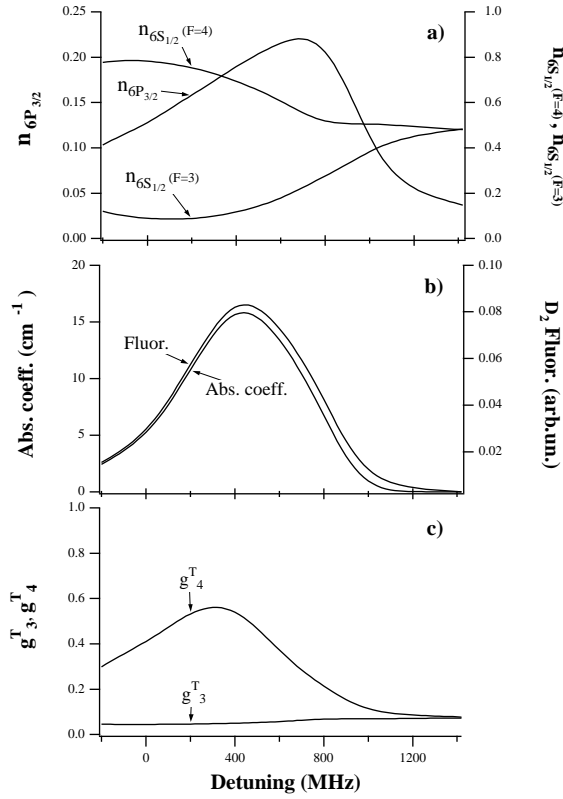


Figure 3. Variables of the theoretical model versus laser detuning at temperature $T = 372$ K and laser intensity $I_L = 0.6 \text{ W cm}^{-2}$ for $6S_{1/2} \rightarrow 6P_{3/2}$ excitation. Laser detuning, in MHz, is measured from the line centre of the $F = 4 \rightarrow F' = 3$ transition. All populations are normalized to the total density of atoms. (a) Populations $n_{6S_{1/2}(F=3)}$, $n_{6S_{1/2}(F=4)}$ in the ground-state hyperfine levels, and population of the upper state $n_{6P_{3/2}}$. (b) Absorption coefficient for the $6S_{1/2} \rightarrow 6P_{3/2}$ transition and the corresponding fluorescence intensity. (c) Trapping factors g_3^T and g_4^T for the group of transitions terminating on the $6S_{1/2}(F = 3)$ and $6S_{1/2}(F = 4)$ levels, respectively.

The laser intensity was taken to be 0.6 W cm^{-2} , which was close to the experimental value. Table 1 reports the values of $n_{6P_{3/2}}/n$, $g_{6P_{3/2}}^T \equiv \Gamma_{6P_{3/2} \rightarrow 6S_{1/2}}^{\text{eff}} / \Gamma_{6P_{3/2} \rightarrow 6S_{1/2}}$, and $G_{7P_{J'}}$, at the laser frequency of maximum $6P_{3/2}$ fluorescence. As the temperature increases from 354 K towards 392 K, the fraction of the population $n_{6P_{3/2}}/n$ increases by a factor of 2, whereas $\Gamma_{6P_{3/2} \rightarrow 6S_{1/2}}^{\text{eff}}$ decreases by about 60%. The $7P_{J'}$ factors $G_{7P_{J'}}$ increase with temperature, the increase being slightly more pronounced on the $7P_{3/2} \rightarrow 6S_{1/2}$ transition. We report also in table 1 (b columns) the same quantities calculated under the assumption that the distribution of population among the various hyperfine sublevels of the $6P_{3/2}$ state is thermalized because of radiation trapping. Calculations labelled a are based upon the opposite assumption that the $6P_{3/2}$ state hyperfine levels retain the population distribution created by the laser pumping. In the thermalized version, the temperature behaviour of all parameters is similar, although values for $n_{6P_{3/2}}$ and $g_{6P_{3/2}}^T$ are lower. We have calculated the frequency positions of the maxima of $6P_{3/2}$ fluorescence, $6P_{3/2}$ population ($7P_{J'}$ fluorescence maximum) and the absorption coefficient, with and without the assumption of thermalization among the upper-state hyperfine levels. We find that the positions of these maxima do not

Table 1. Fractions of population in the excited state and radiation-trapping factors (calculated as the Molisch fundamental (lowest) mode decay rate—see [9, 10]) for different temperatures in the case of $6P_{3/2}$ excitation. a, without thermalization; b, with thermalization assumed among hyperfine sublevels of the excited state.

T (K)	$n_{6P_{3/2}}/n$		$g_{6P_{3/2}}^T$		$G_{7P_{1/2}}$		$G_{7P_{3/2}}$	
	a	b	a	b	a	b	a	b
354	0.147	0.0639	0.592	0.551	1.02	1.02	1.05	1.05
359	0.153	0.0823	0.548	0.504	1.02	1.02	1.06	1.06
363	0.163	0.0995	0.516	0.465	1.03	1.03	1.08	1.07
368	0.175	0.124	0.475	0.415	1.03	1.03	1.10	1.09
372	0.193	0.145	0.425	0.376	1.04	1.04	1.12	1.11
376	0.209	0.167	0.384	0.338	1.05	1.05	1.15	1.14
380	0.225	0.189	0.345	0.303	1.06	1.06	1.17	1.16
384	0.241	0.212	0.309	0.270	1.07	1.07	1.21	1.19
387	0.254	0.229	0.282	0.247	1.08	1.08	1.24	1.22
392	0.270	0.257	0.242	0.213	1.10	1.11	1.29	1.27

change much with temperature and laser intensity under the two assumptions.

Figure 3 reports populations, $6P_{3/2} \rightarrow 6S_{1/2}$ resonance fluorescence, $6S_{1/2} \rightarrow 6P_{3/2}$ absorption coefficient, and trapping factors g_F^T for the $6P_{3/2} \rightarrow 6S_{1/2}$ fluorescence versus laser detuning (with respect to the $F = 4 \rightarrow F' = 3$ transition, in MHz) at a temperature $T = 372$ K and laser intensity $I_L = 0.6$ W cm $^{-2}$. The maximum of the excited state population does not coincide with the maximum of absorption or fluorescence. Figure 4 shows the same quantities as a function of laser intensity near the frequency of maximum fluorescence. It may be noted that the population in the excited state stays constant in the range of laser intensities close to the experimental value $I_L = 0.6$ W cm $^{-2}$ (for very large intensities, the $6P_{3/2}$ state population starts to decrease because of optical pumping). This is a confirmation that the measured values of rate constants should not depend critically on the laser power, within the range used in this experiment. Both $6P_{3/2} \rightarrow 6S$ fluorescence and the absorption coefficient show a saturation behaviour as observed in the experiment and as expected.

In the case of $6P_{1/2}$ excitation, the behaviour of all parameters versus temperature is similar to that in the case of excitation of the $6P_{3/2}$ state. However, the range of temperatures needed to produce useful EP signals was slightly higher when pumping the $6P_{1/2}$ state (even though the EP rate coefficients are larger) because of the following factors: the lower laser power available, the smaller oscillator strength of the $6S_{1/2} \rightarrow 6P_{1/2}$ transition, the greater importance of optical pumping due to the absence of cycling transitions, and shorter effective lifetimes for atoms in the $6P_{1/2}$ state due to a lower radiation trapping probability. In table 2 we give the maximum values of $n_{6P_{1/2}}/n$, $g_{6P_{1/2}}^T \equiv \Gamma_{6P_{1/2} \rightarrow 6S_{1/2}}^{\text{eff}}/\Gamma_{6P_{1/2} \rightarrow 6S_{1/2}}$ and $G_{7P_{1/2}}$, assuming no thermalization among the excited state hyperfine levels. In figure 5 we show the same quantities as in figure 3 versus laser detuning, but for the case of $6P_{1/2}$ excitation, at $T = 384$ K and laser intensity $I_L = 0.25$ W cm $^{-2}$. In this case, the hyperfine sublevels of the $6P_{1/2}$ state are Doppler resolved and there are no ‘closed’ transitions. Thus the laser frequencies that maximize the absorption coefficient, the excited-state population $n_{6P_{1/2}}$, and the resonance fluorescence always coincide near zero detuning. Laser intensities available in this case are lower than for $6P_{3/2}$ excitation, but are still in the region where the various parameters are not critically dependent on the intensity. Figure 6 shows the laser intensity dependence of the various parameters for $6P_{1/2}$ excitation.

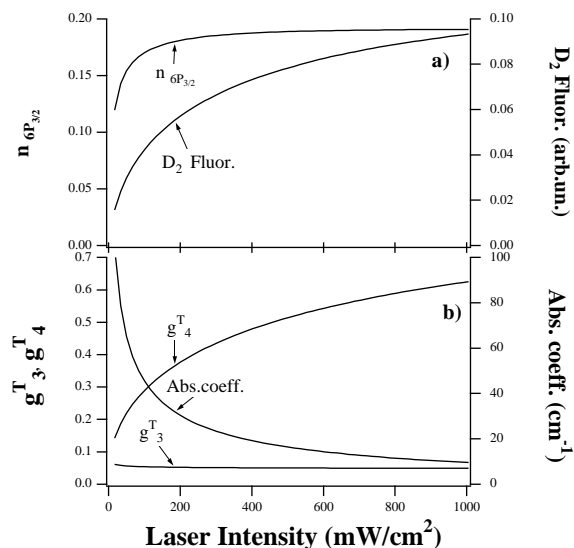


Figure 4. Variables of the theoretical model versus laser intensity at temperature $T = 372$ K and laser frequency detuning of 400 MHz from the $6S_{1/2}(F = 4) \rightarrow 6P_{3/2}(F' = 3)$ transition. (a) Excited-state population and fluorescence intensity. (b) Trapping factors and absorption coefficient.

Table 2. Fractions of population in the excited state and radiation-trapping factors (calculated as the Molisch fundamental (lowest) mode decay rate—see [9, 10]) for different temperatures in the case of $6P_{1/2}$ excitation assuming no thermalization among hyperfine sublevels of the excited state.

T (K)	$n_{6P_{1/2}}/n$	$g_{6P_{1/2}}^T$	$G_{7P_{1/2}}$	$G_{7P_{3/2}}$
368	0.0491	0.233	1.04	1.11
376	0.0625	0.212	1.06	1.16
384	0.0783	0.197	1.09	1.24
392	0.0954	0.185	1.13	1.35
402	0.117	0.176	1.20	1.58
410	0.133	0.170	1.29	1.85

Experimental results for the $k_{7P_{j'}}^{(3/2)}$ and $k_{7P_{j'}}^{(1/2)}$ rate coefficients are summarized in table 3. These values are obtained, from equation (7), using the measured fluorescence intensity ratios. The rate coefficients show a slight dependence on the temperature. In the case of $6P_{3/2}$ excitation, assuming no thermalization of excited hyperfine sublevels, the rate coefficients increase slightly with temperature over the entire interval. When thermalization is assumed, the rate coefficients decrease with T . Presented in [12] is an experimental study of the thermalization of caesium $6P_{1/2}$ and $6P_{3/2}$ state velocity-selected populations and hyperfine-level populations due to the combined processes of radiation trapping and resonance exchange collisions. The experiments of [12] were carried out in a cell of radius 1.05 cm which is much bigger than the capillary cell used in the present experiment. Nevertheless, the results of [12] show that thermalization occurs whenever the probability of reabsorption of resonance photons in the vapour is significant. Thus we believe that the thermalization assumption is valid, for our case, above roughly $T = 370$ K and we therefore

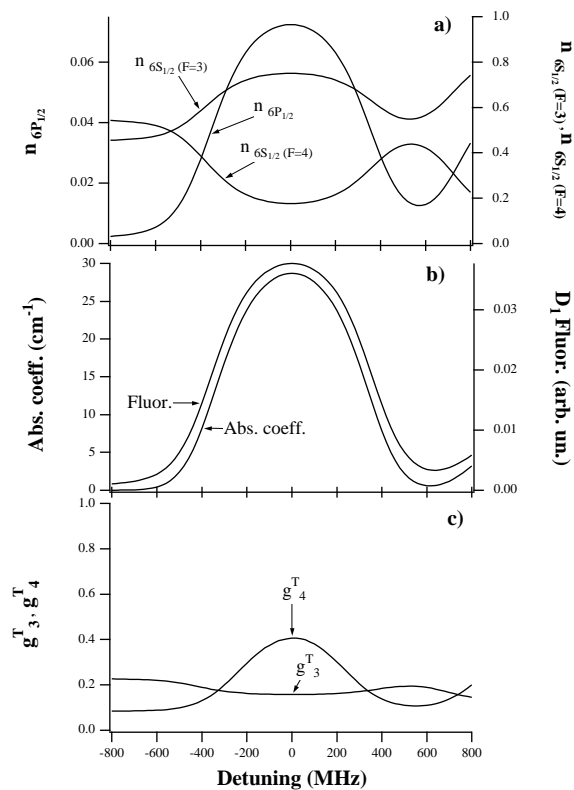


Figure 5. Variables of the theoretical model versus laser detuning at temperature $T = 384$ K and laser intensity $I_L = 0.25 \text{ W cm}^{-2}$ for $6S_{1/2} \rightarrow 6P_{1/2}$ excitation. Laser detuning, in MHz, is measured from the $6S_{1/2}(F = 4) \rightarrow 6P_{1/2}(F' = 3)$ transition (see figure 3 caption for description of the various curves).

average the thermalized values above this temperature with the unthermalized values below to obtain our final reported rate coefficients. Our averaged values for the $7P_{J'}$ EP rate coefficients are given in table 4 for $6P_{3/2}$ and $6P_{1/2}$ excitation.

We now discuss terms neglected in going from equation (2) to equation (4), and the other sources of uncertainty in our final rate-coefficient values. In the sum representing cascade emission we can have contributions to the $7P_{J'}$ population from the $6D_J$ and $8S_{1/2}$ levels. We determine from our observations at higher atom densities, and from the results for the relevant EP rates obtained in [1], that this contribution to the $7P_{J'}$ populations can amount to as much as 10–15% and 40–80% for cascade from the $6D$ and $8S$ levels, respectively, for D_2 pumping, but less than 3% and 1% for D_1 pumping. In the present experiment, a search was made for $8S \rightarrow 6P_J$ fluorescence at 761.1 and 794.6 nm with D_2 pumping, but this could only be observed for temperatures above 410 K. Since the detection system sensitivity is much greater for the blue $7P_{J'} \rightarrow 6S$ fluorescence, this does not preclude a significant $8S$ cascade contribution. However, it is also possible that the $8S$ fluorescence observed here and in the experiment of [1] only at the highest temperatures, is due to sources other than EP collisions. For example, $8S$ might be populated by recombination or excitation transfer collisions involving electrons produced by associative ionization, Penning ionization, or photoionization, but only at the highest temperatures of these experiments. (The absence of

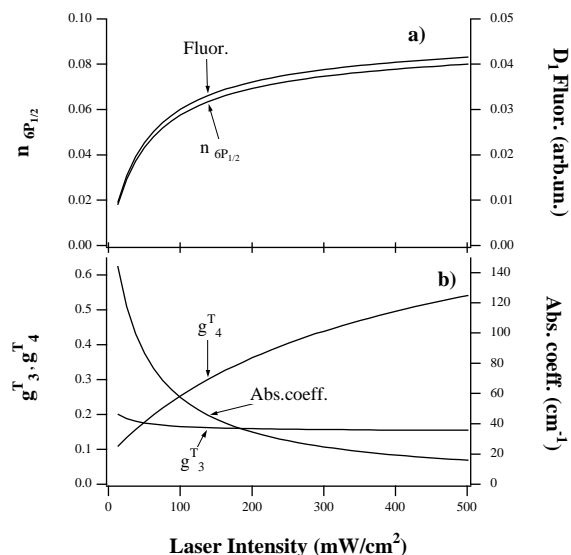


Figure 6. Variables of the theoretical model versus laser intensity at temperature $T = 384$ K and laser frequency resonant with the $6S_{1/2}(F = 4) \rightarrow 6P_{1/2}(F' = 3)$ transition.

fluorescence from other high-lying levels at all but the highest temperatures is evidence that such ionization processes are not important over most of the range of temperatures studied here.) Thus we cannot rule out a significant cascade contribution to our measured values of $k_{7P_{j'}}^{(3/2)}$. In the case of $6P_{3/2}$ excitation, the neglect of $6P_{1/2} + 6P_{1/2}$ EP collisions introduces negligible error in our rate coefficients, but the contribution from $6P_{1/2} + 6P_{3/2}$ collisions can be significant, because the energy deficit is much smaller than for $6P_{3/2} + 6P_{3/2}$ collisions. At present, we cannot estimate this contribution, but this question can be answered by a two-laser experiment to investigate $6P_{1/2} + 6P_{3/2}$ EP collisions which may yield the biggest cross sections. In the case of $6P_{1/2}$ excitation, the rate coefficients are much larger, and we estimate that $6P_{1/2} + 6P_{3/2}$ and $6P_{3/2} + 6P_{3/2}$ collisions will not contribute significantly to the uncertainties. Other sources of uncertainty include the approximate treatment of radiation trapping and relaxation through wall collisions, and the laser detuning dependence of the various model parameters since laser detuning was not carefully monitored. One final source of uncertainty is related to the choice of which theoretical natural radiative rates to use in order to calculate branching factors. These vary significantly between different theoretical calculations found in the literature, [7, 17–30]. In [1] the values given by Warner [7] were chosen because a self-consistent set for all relevant radiative rates was needed. Here we have again chosen to use the values of Warner so that our results can be directly compared with those of [1].

Values in table 4 reflect statistical errors only. We believe that in light of possible systematic errors discussed above, the overall rate coefficients should be considered to be accurate only to within a factor of 2 (excluding the possible systematic 8S contribution to $k_{7P_{j'}}^{(3/2)}$ mentioned above). The current values are also compared in table 4 with the values we obtained in the very different experimental circumstances of [1]. It can be seen that the two sets of results agree, but only to within the rather large combined error bars (systematic as well as statistical) of the two experiments. The fact that this agreement is only marginal is a reflection of the difficulties associated with measurements of this type. However, it

Table 3. EP rate coefficients in the case of $6P_{3/2}$ and $6P_{1/2}$ excitation. a, without thermalization; b, with thermalization assumed among hyperfine sublevels of the excited state. For $6P_{1/2}$ excitation we assume no thermalization takes place. Error bars for $6P_{3/2}$ excitation represent statistical uncertainties as obtained from five independent measurements at each T ; for $6P_{1/2}$ excitation only one measurement was made for each T .

6P _{3/2} excitation				
T (K)	$k_{7P_{3/2}}^{(3/2)}$ (10^{-12} cm ³ s ⁻¹)		$k_{7P_{1/2}}^{(3/2)}$ (10^{-12} cm ³ s ⁻¹)	
	a	b	a	b
354	1.4 ± 0.2	2.9 ± 0.4	1.1 ± 0.2	2.4 ± 0.4
359	1.6 ± 0.2	2.7 ± 0.4	1.5 ± 0.3	2.6 ± 0.5
363	1.8 ± 0.3	2.6 ± 0.5	1.4 ± 0.2	2.1 ± 0.3
368	1.7 ± 0.4	2.1 ± 0.5	1.3 ± 0.2	1.6 ± 0.2
372	1.6 ± 0.2	1.9 ± 0.3	1.8 ± 0.3	2.1 ± 0.4
376	1.6 ± 0.1	1.8 ± 0.1	1.5 ± 0.1	1.7 ± 0.1
380	1.7 ± 0.1	1.8 ± 0.1	1.6 ± 0.1	1.7 ± 0.1
384	1.6 ± 0.4	1.6 ± 0.4	1.3 ± 0.3	1.3 ± 0.3
387	1.5 ± 0.3	1.5 ± 0.3	1.5 ± 0.2	1.4 ± 0.2
392	2.0 ± 0.3	1.9 ± 0.3	1.8 ± 0.3	1.7 ± 0.3
6P _{1/2} excitation				
T (K)	$k_{7P_{3/2}}^{(1/2)}$ (10^{-11} cm ³ s ⁻¹)		$k_{7P_{1/2}}^{(1/2)}$ (10^{-11} cm ³ s ⁻¹)	
368	1.4 ± 0.7		3.1 ± 0.9	
376	1.7 ± 0.7		3.0 ± 0.9	
384	1.5 ± 0.7		3.6 ± 0.9	
392	1.7 ± 0.7		3.1 ± 0.9	
402	2.0 ± 0.7		3.7 ± 0.9	
410	3.2 ± 0.7		5.3 ± 0.9	

Table 4. Averaged values of EP rate coefficients. a, average of unthermalized values. b, average of unthermalized values from $T = 354$ K to $T = 368$ K and thermalized values from $T = 372$ K to $T = 392$ K. c, results of [1]. Errors represent statistical uncertainties only. In light of possible systematic errors (see text) we believe the present rate coefficients are only accurate to within a factor of 2, while those of [1] are accurate to approximately ±50%.

6P _{3/2} excitation					
$k_{7P_{3/2}}^{(3/2)}$ (10^{-12} cm ³ s ⁻¹)			$k_{7P_{1/2}}^{(3/2)}$ (10^{-12} cm ³ s ⁻¹)		
a	b	c	a	b	c
1.72 ± 0.05	1.65 ± 0.05	6.1 ± 3.1	1.52 ± 0.05	1.60 ± 0.04	5.9 ± 3.1
6P _{1/2} excitation					
$k_{7P_{3/2}}^{(1/2)}$ (10^{-11} cm ³ s ⁻¹)			$k_{7P_{1/2}}^{(1/2)}$ (10^{-11} cm ³ s ⁻¹)		
a	c		a	c	
1.9 ± 0.3	4.5 ± 1.4		3.6 ± 0.3	13.0 ± 6.0	

also indicates that the overall quoted errors are reasonable.

Finally, we should comment on the experiment recently reported by Vadla *et al* [31], who used an original method to avoid radiation trapping. In that work, the dipole forbidden

6S \rightarrow 5D transition of caesium at 685 nm was pumped with a cw dye laser and EP collisions $6P + 6P \rightarrow 6D + 6S$, $6P + 5D \rightarrow 7D + 6S$, and $5D + 5D \rightarrow 7F + 6S$ were observed. The excited-atom density was measured directly using a probe laser as in [1]. In addition, complicated radiation-trapping calculations (or equivalently calculations of transmission factors as in [1]) were cleverly avoided by measuring the ratio of fluorescence from the high-lying state produced through EP to fluorescence emitted in the optically thin line wing of the self-broadened resonance line. The latter must be carefully calibrated, but this can be done using theory. However, due to the pumping mechanism, fine-structure effects (i.e. differences between rates for $6P_{3/2} + 6P_{3/2}$ vs $6P_{1/2} + 6P_{1/2}$ collisions) could not be studied in [31]. The present work also differs from [31] in the product states under investigation ($7P_{J'}$ against 6D, 7D, and 7F). We note that due to the different temperature ranges of the two experiments and the lack of fine-structure selection in [31], those results also cannot be compared in detail with the $6P_J + 6P_J \rightarrow 6D_{J'} + 6S_{1/2}$ rate coefficients of [1]. However, the cross section for $6P + 6P \rightarrow 6D + 6S$ (9.5×10^{-15} cm²) reported in [31] is certainly consistent with the values 1.3×10^{-14} , 8.0×10^{-15} , 2.7×10^{-15} , and 5.6×10^{-15} cm² obtained in [1] for the process $6P_J + 6P_J \rightarrow 6D_{J'} + 6S_{1/2}$ with ($J = 1/2, J' = 3/2$), ($J = 1/2, J' = 5/2$) ($J = 3/2, J' = 3/2$) and ($J = 3/2, J' = 5/2$), respectively.

5. Conclusions

We have presented the results of an experimental study of $\text{Cs}(6P_J) + \text{Cs}(6P_J) \rightarrow \text{Cs}(7P_{J'}) + \text{Cs}(6S_{1/2})$ EP collisions. The experiment was carried out in a capillary cell using diode laser excitation, thus simplifying the analysis of the radiation-trapping problem. However, because the excited-atom density could not be measured directly in this experiment, we have also developed a model to estimate the population of $\text{Cs}(6P_J)$ atoms excited by a cw single-mode laser under conditions of saturation, radiation trapping and hyperfine optical pumping. The last two effects are particularly difficult to incorporate into the model since each affects the other. Thus a self-consistent solution to the optical pumping/radiation trapping problem was developed by iteration. We believe this is the first such model to successfully incorporate these simultaneous effects. The model results were combined with measured fluorescence ratios to obtain the EP rate coefficients. The quantitative results are in agreement with those obtained in very different experimental conditions [1], but only within the combined large error bars of the two experiments (including systematic errors). Nevertheless, we believe these results are useful since they corroborate the results of [1], which is gratifying in this field where different measurements of the same rates sometimes yield discrepancies of several orders of magnitude. Moreover, our theoretical model and its application to the study of EP in caesium highlights the complications which arise in the experimental study of excited atom–excited atom collisions, especially in a heavy system such as caesium. In addition, we have been able to confirm that $6P_{1/2} + 6P_{1/2}$ collisions are much more effective than $6P_{3/2} + 6P_{3/2}$ collisions at populating the $7P_{J'}$ levels. Our results obtained with D_1 pumping also demonstrate that $7P_{1/2}$ is about two times more likely to be populated than $7P_{3/2}$, while the two $7P_{J'}$ levels are approximately equally populated when D_2 pumping is employed. This supports the idea that not only energy deficits but also angular momentum can be important in some circumstances for EP processes. Additional evidence could be obtained from an experiment designed to study mixed $6P_{3/2} + 6P_{1/2}$ collisions with simultaneous laser excitation of the $6P_{3/2}$ and $6P_{1/2}$ levels. Rate coefficients for the $6P_{3/2} + 6P_{1/2}$ entrance channel are likely to be larger than those for either the $6P_{1/2} + 6P_{1/2}$ or $6P_{3/2} + 6P_{3/2}$ channels studied here and in [1].

Acknowledgments

SM undertook this work with the support of the Program for Training and Research in Italian Laboratories of ICTP, Trieste, Italy. We are grateful to Professor T Yabuzaki for lending us a diode laser operating at 895 nm and to M Badalassi for preparing the capillary cells. This work is partially supported by the EEC Network grant ERBCHRXCT 930344, and by NSF grant PHY-9119498. Finally, we would like to thank the referees for constructive criticisms and valuable suggestions for improving the text.

References

- [1] Jabbour Z J, Namiokta R K, Huennekens J, Allegrini M, Milošević S and de Tomasi F 1996 *Phys. Rev. A* **54** 1372
- [2] Milošević S, de Tomasi F, Fuso F and Allegrini M 1995 *Europhys. Lett.* **32** 703
- [3] Allegrini M, Bicchi P and Moi L 1983 *Phys. Rev. A* **28** 1338
- [4] Nesmeyanov A N 1963 *Vapor Pressure of the Elements* (New York: Academic)
- [5] Stair R, Schneider W E and Jackson J K 1963 *Appl. Opt.* **2** 1151
- [6] Pace P W and Atkinson J B 1974 *Can. J. Phys.* **52** 1641
- [7] Warner B 1968 *Mon. Not. R. Astron. Soc.* **139** 115
- [8] Czajkowski M and Krause L 1965 *Can. J. Phys.* **43** 1259
- [9] Molisch A F, Oehry B P, Schupita W and Magerl G 1993 *J. Quant. Spectrosc. Radiat. Transfer* **49** 361
- [10] Molisch A F, Oehry B P and Magerl G 1992 *J. Quant. Spectrosc. Radiat. Transfer* **48** 377
- [11] Sagle J, Namiokta R K and Huennekens J 1996 *J. Phys. B: At. Mol. Opt. Phys.* **29** 2629
- [12] Huennekens J, Namiokta R K, Sagle J, Jabbour Z J and Allegrini M 1995 *Phys. Rev. A* **51** 4472
- [13] de Tomasi F, Allegrini M, Arimondo E, Agarwal G S and Ananthalakshmi P 1993 *Phys. Rev. A* **48** 3820
- [14] Chen C L and Phelps A V 1968 *Phys. Rev.* **173** 62
- [15] Vuletić V, Sautenkov V A, Zimmermann C and Hänsch T W 1993 *Opt. Commun.* **99** 185
- [16] Arditi M, Hirano I and Tougne P 1978 *J. Phys. D: Appl. Phys.* **11** 2465
- [17] Heavens O S 1961 *J. Opt. Soc. Am.* **51** 1058
- [18] Stone P M, 1962 *Phys. Rev.* **127** 1151
- [19] Anderson E M and Zilitis V A 1964 *Opt. Spectrosc.* **16** 211
- [20] Weisheit J C 1972 *Phys. Rev. A* **5** 1621
- [21] Norcross D W 1973 *Phys. Rev. A* **7** 606
- [22] Fabry M, 1976 *J. Quant. Spectrosc. Radiat. Transfer* **16** 127
- [23] Fabry M and Cussenot J R 1976 *Can. J. Phys.* **54** 836
- [24] Lindgard A and Nielsen S E 1977 *At. Data Nucl. Data Tables* **19** 533
- [25] Laplanche G, Jaouen M and Rachman A 1983 *J. Phys. B: At. Mol. Phys.* **16** 415
- [26] Martin I and Barrientos C 1986 *Can. J. Phys.* **64** 867
- [27] Martin I and Barrientos C 1987 *Can. J. Phys.* **65** 435
- [28] Migdalek J and Wyrozumska M 1987 *J. Quant. Spectrosc. Radiat. Transfer* **37** 581
- [29] Liaw S S 1992 *Can. J. Phys.* **70** 1279
- [30] Theodosiou C E 1984 *Phys. Rev. A* **30** 2881 and references therein
- [31] Vadla C, Niemax K and Brust J 1996 *Z. Phys. D* **37** 241